Title

BIN1 Induces the Formation of T-Tubules and Adult-Like Ca^{2+} Release Units in Developing Cardiomyocytes.

Journal

Stem cells (Dayton, Ohio), 37(1)

ISSN

1066-5099

Authors

De La Mata, Ana
Tajada, Sendoa
O'Dwyer, Samantha
et al.

Publication Date

2019

DOI

10.1002/stem.2927

Peer reviewed

STEM CELLS®

EMBRYONIC STEM CELLS/INDUCED PLURIPOTENT STEM CELLS

BIN1 Induces the Formation of T-Tubules and Adult-Like Ca^{2+} Release Units in Developing Cardiomyocytes

ANA DE LA MATA,[a] SENDOA TAJADA,[a] SAMANTHA O'DWYER,[a] COLLIN MATSUMOTO,[a] ROSE E. DIXON,[a] NIRMALA HARIHARAN,[b] CLAUDIA M. MORENO,[a] LUIS FERNANDO SANTANA[a]

Key Words. hESC • Cardiac myocytes • BIN1 • T-tubules • $Ca_V1.2$ • Calcium release units

[a]Department of Physiology & Membrane Biology, University of California School of Medicine, Davis, California, USA; [b]Department of Pharmacology, University of California School of Medicine, Davis, California, USA

Correspondence: Claudia M. Moreno, Ph.D., Department of Physiology & Membrane Biology, University of California School of Medicine, Davis, California 95616, USA. Telephone: 530-752-8836; e-mail: cmmoreno@ucdavis.edu; or Luis Fernando Santana, Ph.D., Department of Physiology & Membrane Biology, University of California School of Medicine, Davis, California 95616, USA. Telephone: 530-752-8836; e-mail: lfsantana@ucdavis.edu

Received March 16, 2018; accepted for publication September 22, 2018; first published online in STEM CELLS *EXPRESS* October 23, 2018.

http://dx.doi.org/10.1002/stem.2927

ABSTRACT

Human embryonic stem cell-derived cardiomyocytes (hESC-CMs) are at the center of new cell-based therapies for cardiac disease, but may also serve as a useful in vitro model for cardiac cell development. An intriguing feature of hESC-CMs is that although they express contractile proteins and have sarcomeres, they do not develop transverse-tubules (T-tubules) with adult-like Ca^{2+} release units (CRUs). We tested the hypothesis that expression of the protein BIN1 in hESC-CMs promotes T-tubules formation, facilitates $Ca_V1.2$ channel clustering along the tubules, and results in the development of stable CRUs. Using electrophysiology, $[Ca^{2+}]_i$ imaging, and super resolution microscopy, we found that BIN1 expression induced T-tubule development in hESC-CMs, while increasing differentiation toward a more ventricular-like phenotype. Voltage-gated $Ca_V1.2$ channels clustered along the surface sarcolemma and T-tubules of hESC-CM. The length and width of the T-tubules as well as the expression and size of $Ca_V1.2$ clusters grew, as BIN1 expression increased and cells matured. BIN1 expression increased $Ca_V1.2$ channel activity and the probability of coupled gating within channel clusters. Interestingly, BIN1 clusters also served as sites for sarcoplasmic reticulum (SR) anchoring and stabilization. Accordingly, BIN1-expressing cells had more $Ca_V1.2$-ryanodine receptor junctions than control cells. This was associated with larger $[Ca^{2+}]_i$ transients during excitation–contraction coupling. Our data support the view that BIN1 is a key regulator of T-tubule formation and $Ca_V1.2$ channel delivery. By studying the role of BIN1 during the differentiation of hESC-CMs, we show that BIN1 is also important for $Ca_V1.2$ channel clustering, junctional SR organization, and the establishment of excitation–contraction coupling. STEM CELLS *2019;37:54–64*

SIGNIFICANCE STATEMENT

Human embryonic stem cell-derived cardiomyocytes (hESC-CMs) express contractile proteins and sarcomeres and have been successfully implemented in preclinical studies to treat heart disease. However, they lack the ability to develop T-tubules and thus differ from mature functional cardiomyocytes. This study demonstrates that BIN1 increases differentiation of hESC to ventricular-like cardiomyocytes by regulating the formation of T-tubules and adult-like Ca^{2+} release units, thus resulting in the induction of functional dyads of hESC-CMs. The study provides insight into the biogenesis of T-tubules and Ca^{2+} release units in cardiac cells and suggest strategies for the generation of cells that could prove to be better suited for ESC-based cardiac regenerative therapy.

INTRODUCTION

Human embryonic stem cell-derived cardiomyocytes (hESC-CMs) have the dual promise of being used for cell-based therapies to combat cardiac diseases [1–3] and as a model for cardiac cell development. For these cell-based therapies to be successful, it is imperative that the transplanted cells integrate with the host cells to improve cardiac function. They must therefore bear a close structural and functional resemblance to mature cardiomyocytes. For example, to treat an infarcted left ventricle, one would ideally transplant hESC-CMs that have matured into cells possessing a transverse-tubule (T-tubule) network, which is essential for excitation–contraction (EC) coupling in adult ventricular myocytes.

T-tubules extend to the interior of the cell providing the structural platform for the formation of Ca^{2+} release units (CRUs). These are specialized regions where clusters of sarcolemmal voltage-gated $Ca_V1.2$ channels are in close juxtaposition (≈15 nm) to ryanodine receptors (RyRs) in the

junctional sarcoplasmic reticulum (jSR) [4, 5]. Yet, although hESC-CMs express contractile proteins and have sarcomeres, they do not normally develop T-tubules with CRUs. Maturation of hESC-CMs with adult-like T-tubules and CRUs could provide a useful human model for pathological EC coupling-related conditions. In addition, observation of this maturation process offers a unique opportunity to study the mechanisms controlling the formation of signature cardiac structures such as T-tubules and dyads, which are incompletely understood.

Several proteins have been identified as key players in T-tubule biogenesis and subsequent dyad formation. These include, caveolin-3 (CAV3) [6–8], dysferlin [9, 10], junctophilin 2 (JPH2) [11], triadin [12], and BIN1 (also known as Amphiphysin 2) [13–15]. Of these proteins, BIN1, a member of the Bin1-Amphiphysin-Rvs domain superfamily, is of particular interest since it has not only been implicated in T-tubule biogenesis, in its role as a membrane curvature-generating molecule, but it has also been reported to act as an anchor point for microtubules in cardiac muscle, where it colocalizes with, and facilitates trafficking of $Ca_V1.2$ channels to the sarcolemma [13–15]. However, whether BIN1 is directly implicated in the formation of $Ca_V1.2$ clusters and sarcolemmal-SR dyads in developing myocytes is unclear.

Clustering of $Ca_V1.2$ channels along the surface sarcolemma and T-tubule network is important, as the physical proximity of channels within the clusters allows dynamic allosteric interactions that permit cooperative gating activity of the channels, resulting in amplification of Ca^{2+} entry during EC coupling [16, 17]. Dixon et al. [16] proposed that $Ca_V1.2$ channel-to-channel coupling is initiated when membrane depolarization opens $Ca_V1.2$ channels, allowing a small amount of Ca^{2+} to enter the cell. The incoming Ca^{2+} binds to calmodulin, thereby promoting physical coupling of adjacent channels via the pre-IQ (isoleucine-glutamine) domains located in the C-terminal of the channels. Physical contact increases the activity of adjoined channels. As individual channels within a cluster inactivate and close, $[Ca^{2+}]_i$ decreases and coupling dissolves. A key tenet of this model is that the overall activity of $Ca_V1.2$ channels within a cluster depends on the number of channels that couple. Clustering of $Ca_V1.2$ channels could also directly regulate the coupling strength with RyRs conferring stability to the dyads. At present, however, the mechanisms regulating $Ca_V1.2$ channel cluster formation and maintenance are poorly understood.

In this study, we evaluated the effect of BIN1 expression in the differentiation of hESC-CM. We evaluated changes in the electrical phenotype, the biogenesis of T-tubules, and the effect on $Ca_V1.2$ clustering, and dyad establishment. Our data show that: (a) BIN1 overexpression favors the differentiation of hESC to a more ventricular-like phenotype; (b) BIN1 promotes the progressive formation of T-tubules during hESC-CMs differentiation; (c) BIN1 has a direct effect on $Ca_V1.2$ channel clustering and increases $Ca_V1.2$ channel activity; and (d) hESC-CM expressing BIN1 also exhibit stable dyads and more synchronized SR Ca^{2+} release during EC coupling.

Materials and Methods

hESCs (WiCell Line WA09) were differentiated into CMs using a modified version of the directed-differentiation protocol described by Palpant et al. [18]. We generated two lentiviruses for this study; the first one contained the plasmid pDEST/N1-hBIN1-GFP (Addgene, 27305)14, encoding the human BIN1 transcript variant 8 tagged with green fluorescent protein (EGFP). The second lentivirus contained red fluorescent protein (RFP) with an N-terminal calreticulin signal sequence and a C-terminal endoplasmic reticulum (SR) retention signal (lysine, aspartic acid, glutamic acid, and leucine, KDEL). Infections were performed on undifferentiated hESCs (before starting the differentiation protocol) by adding the corresponding lentivirus (1×10^7 pfu/ml, 10 multiplicity of infection (MOI)) in the presence of 6 μg/ml of polybrene for 18 hours. Successful infection was assessed by GFP and RFP fluorescence detection after 72 hours. A detailed version of the "Materials and Methods" section can be found in the Supporting Information online.

Results

Expression of BIN1 Induces the Formation of T-Tubules in hESC-CMs

We began our investigation by imaging living, control and BIN1-EGFP-expressing hESC-CMs at 10 (differentiation days [DD] 10), 20 (DD20), and 30 days (DD30) after the induction of cardiomyocyte differentiation (Fig. 1). Immunoblot and densitometric analyses confirmed expression of exogenous BIN1 and GFP in hESC-CM transduced with BIN1-EGFP lentivirus. Levels of exogenous BIN1 and GFP, but not endogenous BIN1, increased at DD20 and DD30 relative to DD10 (Supporting Information Fig. S1). Cell shape was characterized as described previously [19]. No significant differences in length/width ratio or cell roundness were observed between BIN1-transduced and control hESC-CMs at DD10, DD 20, or DD 30 (Supporting Information Fig. S2). The goal of these experiments was to test the hypothesis that BIN1 binds to the membrane and creates invaginations that grow in diameter and depth as hESC-CMs differentiate and mature (Fig. 1A). Figure 1B shows confocal sections of representative control and BIN1-EGFP hESC-CMs. The voltage-sensitive plasma membrane dye Di-8-ANEPPS was used to visualize the contours of the sarcolemma of these cells. In control cells, Di-8-ANEPPS fluorescence was confined to the periphery of the cells with no detectable signs of membrane invaginations at all differentiation days. Consistent with our hypothesis, in cells transduced with BIN1-EGFP there were prominent T-tubule-like structures that radiated toward the center of the cell and where BIN1 was localized.

Figure 1C shows a three-dimensional reconstruction of a Z-stack of images from a hESC-CM expressing BIN1-EGFP. Note that BIN1-EGFP was expressed throughout the membrane surface forming tubules that varied in diameter and length through the cell. BIN1-EGFP tubules were detected even 10 days after the initiation of cardiac differentiation. T-tubules length was manually measured in BIN1-hESC-CMs at DD10, DD20, and DD30. Although, on average, the number of BIN1-EGFP tubules per cell did not change over time, both the diameter (DD10 = 0.2 ± 0.02 μm; DD20 = 0.28 ± 0.02 μm; DD30 = 0.5 ± 0.04 μm) and length (DD10 = 2.25 ± 0.2 μm; DD20 = 3.80 ± 0.4 μm; DD30 = 7.5 ± 1.1 μm) of tubules increased as cells differentiated (Fig. 1D). Accordingly, cell progressively increased in BIN1-EGFP, but not in control cells over a period of 30 days (Supporting Information Fig. S3). Assuming a specific capacitance of 0.9 $\mu F/cm^2$ for both control and BIN1 groups [20, 21], this translates into an increase in membrane

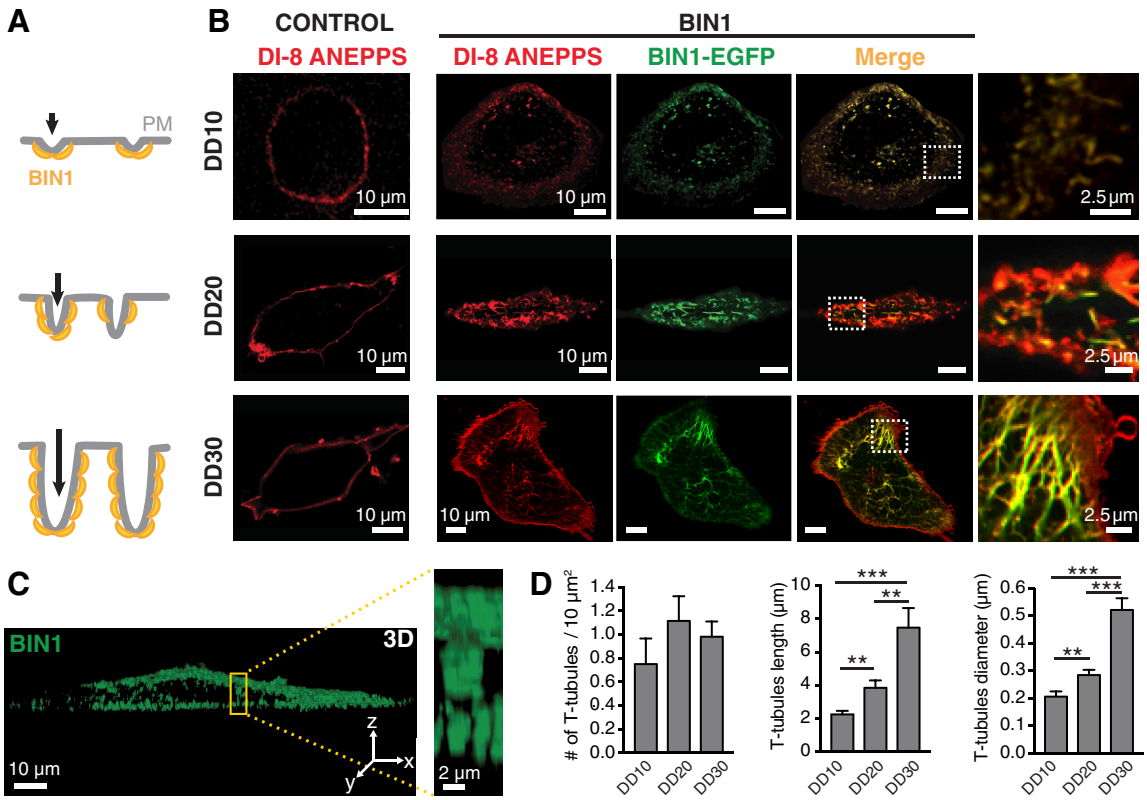

Figure 1. BIN1 expression promotes the formation of T-tubules in human embryonic stem cell-derived cardiomyocyte (hESC-CM). **(A):** Schematic representation of the formation and maturation of T-tubules at differentiation days (DD) 10, DD20, and DD30 in hESC-CM transduced with BIN1-EGFP. **(B):** Representative confocal images of Di-8-ANEPPS labeled membrane (red) in control (left) and BIN1 hESC-CM (right). Additional right panels show the expression pattern of BIN1-EGFP (green). Colocalization of Di-8-ANEPPS and BIN1 appears as yellow in the merged images. Zoom in right panels show with more detail the organization of the tubular structures. **(C):** Front orthogonal view of a Airyscan 3D reconstruction of a hESC-CM BIN1 cell. Zoom-in at the right shows the projection of T-tubules from the top to the bottom of the cell. **(D):** T-tubules density, length and diameter at DD10, DD20, and DD30 in hESC-CM BIN1 cells, n = 4 cells/group. Bars are averages ± SEM. *, $p < .05$; **, $p < .01$; ***, $p < .001$.

surface area of BIN1-EGFP cells from 238 ± 12 µm^2 at DD10 to 374 ± 23 µm^2 at DD30.

In adult ventricular myocytes, T-tubules are organized in a periodic pattern approximately every 1.8 µm, where they flank the sarcomere Z-discs. Supporting Information Figure S4 shows confocal images of sarcomeric α-actinin and BIN1 in fixed and permeabilized DD10, DD20, and DD30 hESC-CMs. hESC-CMs expressed α-actinin as early as 10 days after differentiation (Supporting Information Fig. S4A). To quantify α-actinin and BIN1 organization, we used the TTorg plugin [22] for ImageJ. Briefly, this analysis involves a Fast Fourier Transform (FFT) analysis of α-actinin and BIN1 images, which are converted into a frequency domain that quantifies periodicity. The first harmonic of α-actinin, is the strongest periodicity of the Z-disk network based upon the spacing between each harmonic.

Frequency histograms of α-actinin periodicity were fit with Gaussian functions. At DD10, α-actinin distribution could be fit with the sum of two Gaussian functions with centers at 1.1 ± 0.1 µm and 1.4 ± 0.2 µm (Supporting Information Fig. S4B, S4C). At DD20, α-actinin distribution was also bimodal, but the amplitude of the first peak decreased from 22.1 ± 0.02 at DD10 to 15.2 ± 0.01 at DD20, while the center of the second peak shifted to 1.7 ± 0.2 µm. By DD30, however, the population of α-actinin structures could be fit by a single Gaussian function with a center at 1.7 ± 0.2 µm. These results suggest that the α-actinin organization and the periodicity are increasing along the cell maturation.

Notably, although in some regions BIN1 tubules aligned and ran parallel to α-actinin, in most cells, T-tubules ran perpendicular or diagonal to Z-line structures (Supporting Information Fig. S4A). Indeed, our FFT analysis showed that BIN1 was most frequently found at periods of approximately 0.5 µm in DD10 (0.68 ± 0.20 µm), DD20 (0.56 ± 0.16 µm), and DD30 (0.49 ± 0.20 µm) cells (Supporting Information Fig. S4B, S4C). Interestingly, in a small percentage of subcellular domains (~10%) in DD30, BIN1 tubules were located, like Z-disks, 1.7 ± 0.04 µm apart. In combination, these data suggest that although BIN1 promotes the formation of a periodic tubular network in hESC-CMs, in the vast majority (~90%) of sarcomeres, it does not organize so that tubules flank Z-disks at least 30 days after differentiation.

Expression of BIN1 Promotes Ventricular-like Action Potentials in hESC-CMs

Action potentials (APs) were recorded from spontaneously beating control and hESC-CMs expressing BIN1-EGFP at DD20 and DD30 (Fig. 2). APs were categorized as ventricular, atrial, and nodal-like based on their amplitude and AP shape. Ventricular APs are characterized by a longer duration and a plateau phase, which can be described using a ratio between the

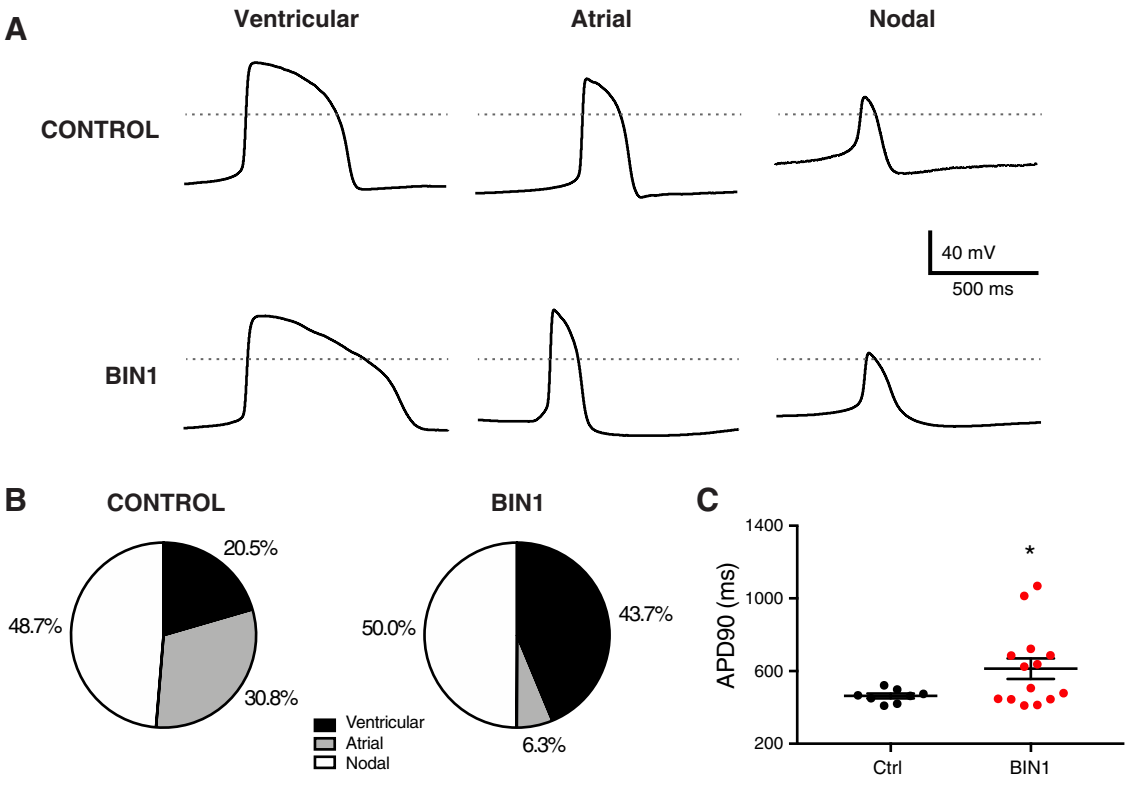

D

AP (n = 69)	Peak (mV)		Rate (bpm)		Amplitude (mV)		MDP (mV)		APD90 (ms)		APD30-40/APD70-80	
	Ctrl	BIN1	Ctrl	BIN1	Ctrl	BIN1	Ctrl	BIN1	Ctrl	BIN1	Ctrl	BIN1
Ventricular-like (n = 22)	44.6 ± 3.1	36.2 ± 2.3	30.3 ± 7.1	17.1 ± 4.0	114.6 ± 2.4	106.1 ± 2.2	-70.0 ± 2.4	-70.4 ± 1.4	463.1 ± 13.1	613.1 ± 56.7	2.0 ± 0.3	2.1 ± 0.3
Atrial-like (n = 14)	38.8 ± 5.2	48.2 ± 3.0	26.9 ± 5.5	12.0 ± 2.0	109.6 ± 4.8	110.9 ± 4.9	-70.0 ± 1.5	-60.8 ± 9.9	312.8 ±19.5	260.8 ± 75.0	1.5 ±0.2	1.2 ± 0.3
Nodal-like (n = 34)	21.8 ± 3.0	19.3 ± 2.8	27.6 ± 4.7	26.1 ± 4.1	85.3 ± 3.2	83.2 ± 3.3	-63.6 ± 1.3	-64.2 ± 2.4	219.6 ± 16.7	215.6 ± 25.3	0.8 ± 0.1	0.9 ± 0.1

Figure 2. BIN1 expression increases ventricular-like phenotype in human embryonic stem cell-derived cardiomyocyte (hESC-CM). **(A):** Representative ventricular-, atrial- and nodal-like action potentials (APs) in control and BIN1 hESC-CM. **(B):** Proportion of each electrical phenotype in control (n = 39) and BIN1 hESC-CM (n = 32). **(C):** Comparison of the action potential duration at 90% of repolarization (ADP90) in control and BIN1 ventricular-like hESC-CM (*, p < .05). **(D):** Summary of AP parameters in control and BIN1 hESC-CM. Abbreviations: MDP, maximum diastolic potential; ADP, action potential duration at the specified percentage of repolarization. Data in the table in panel D are presented as mean ± SEM.

AP duration at 30%–40% and 70%–80% repolarization (i.e., APD30-40/APD70-80) [23]. Cells with a ratio >1.8 and amplitude >100 mV were considered as ventricular-like. Cells with ratios <1.8 and amplitude >100 mV were classified as atrial-like, while cells with ratio <1.8 and amplitude <100 mV were classified as nodal-like. With a few exceptions, cells were easily classified into the three groups using these criteria. There were a few cells that had amplitudes <100 mV but exhibited a clear plateau phase. They were classified as ventricular cardiomyocytes.

Using these criteria, we found that BIN1 expression significantly increases the percentage of ventricular-like CM (43.7% vs. 20.5% in control cells, p = .036) and reduces the percentage of atrial-like cells (6.3% vs. 30.8% in control cells, p = .0104). BIN1 expression did not affect the proportion of cells with a nodal-like phenotype (50.0% vs. 48.7% in control cells, p = .9138; Fig. 2A, 2B)). Interestingly, when we compared ventricular-like APs from control and hESC-CMs expressing BIN1 we observed a significant increase in AP duration (APD90 = 463.1 ± 13.1 ms in control vs. 613.1 ± 56.7 in BIN1 hESC-CMs. p = .038 n = 22; Fig. 2C). All the AP parameters measured are summarized in Figure 2D.

Corroborating with AP data, expression of cardiac ventricular and slow twitch skeletal isoform of myosin light chain-2 (MLC-2V) increases in BIN1-hESC-CMs at DD30 (Supporting Information Fig. S5A, S5B). Additionally, testing the expression of troponin-I (TnI) using TI-4 antibody [24] demonstrated increase in cardiac TnI levels in BIN1-hESC-CMs at DD30 (Supporting Information Fig. S5A, S5C), consistent with previous findings reporting induction of cardiac TnI following several days of spontaneous contraction in mouse ESC-CMs [25]. Collectively the data suggest that BIN1 overexpression increases the portion of ventricular CMs.

BIN1 Expression Increases $Ca_V1.2$ Channels Clustering in hESC-CMs

Reductions of BIN1 have been associated with impairments of $Ca_V1.2$ trafficking and consequently a decrease of $Ca_V1.2$ expression in the sarcolemma of failing ventricular myocytes [26]. Furthermore, increases in $Ca_V1.2$ amplitude and coupling

have been linked to AP prolongation [27]. Thus, we investigated the relationship between BIN1 expression and $Ca_V1.2$ channels clustering and density in hESC-CMs (Fig. 3). Figure 3A shows a three-dimensional (3D) super resolution image of $Ca_V1.2$ and BIN1 at DD30. A movie of one of these 3D images is in the Supporting Information (Supporting Information Video S1). Note that $Ca_V1.2$ channels clustered adjacent to BIN1 in T-tubules. Figure 3B shows 2D super resolution images from DD10, DD20, and DD30 cells. At DD10, BIN1, and $Ca_V1.2$ channels were primarily expressed into small clusters along the surface membrane of the cells. By DD20, when T-tubules were more prominent, a larger (~3.6-fold increase) proportion $Ca_V1.2$ clusters could be detected with an overlapping BIN1 cluster or tubule. In DD30 cells, we saw multiple colocalization patterns emerge: small overlapping clusters of similar size; small $Ca_V1.2$ clusters along BIN1 T-tubules; and large $Ca_V1.2$ clusters spanning the length of a BIN1 T-tubule (Fig. 3B, bottom). The mean $Ca_V1.2$ cluster area was larger in BIN1-expressing cells than in control cells at all ages and BIN1 cluster size was significantly larger after DD20 (Fig. 3C).

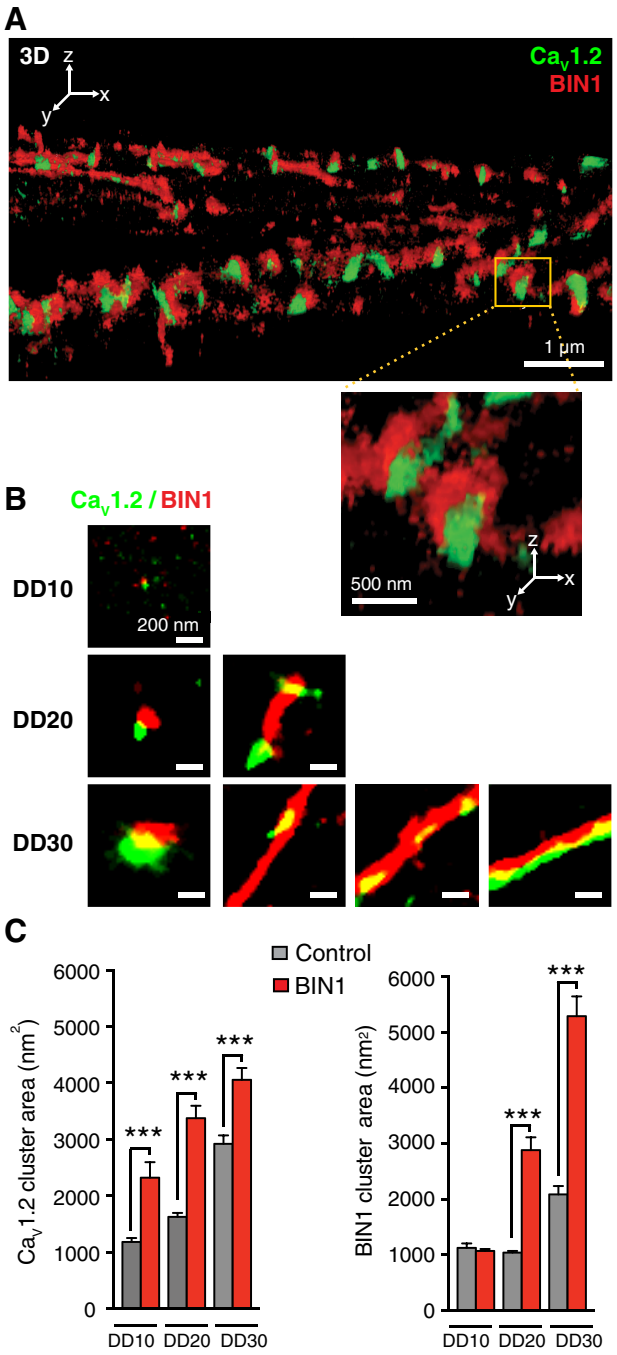

Figure 3. BIN1 increases $Ca_V1.2$ channel clustering in human embryonic stem cell-derived cardiomyocyte (hESC-CM). **(A):** 3D reconstruction of GSD super-resolution images from a representative differentiation days (DD) 30 BIN1 hESC-CM immunostained against $Ca_V1.2$ (green) and BIN1 (red). ROI outlined in yellow and enlarged at the bottom show juxtapositioning of $Ca_V1.2$ and BIN1 clusters. **(B):** Representative GSD 2D super-resolution images of typical $Ca_V1.2$ and BIN1 cluster organizations observed in BIN1 hESC-CMs at DD10, DD20 and DD30. **(C):** $Ca_V1.2$ and BIN1 cluster mean area plots (n = 4 cells/group). Bars are averages ± SEM. ***, $p < .001$.

BIN1 Increases the Activity and Cooperative Gating of Clustered $Ca_V1.2$ Channels in hESC-CM

We tested the hypothesis that the changes in $Ca_V1.2$ clustering induced by BIN1 expression increase the activity of these channels. To do this, we recorded macroscopic $Ca_V1.2$ currents (I_{Ca}) in control and BIN1 cells. Consistent with our hypothesis, we found that I_{Ca} density was significantly higher in BIN1 than in control cells at DD10 (I_{Ca} density at 0 mV, 19.1 ± 2.1 pA/pF vs. 12.2 ± 0.8 pA/pF, p = .0052), DD20 (at 0 mV, 21.5 ± 1.4 pA/pF vs. 11.6 ± 1.0 pA/pF, $p < .0001$), and DD30 (at 0 mV, 21.1 ± 1.8 pA/pF vs. 9.2 ± 1.4 pA/pF, $p < .0001$), respectively (Fig. 4A, 4C)).

I_{Ca} is related to the number (N) of functional $Ca_V1.2$ channels in the surface membrane, their open probability (P_o), and the amplitude of their unitary currents (i_{Ca}) by the equation $I_{Ca} = NP_oi_{Ca}$. Thus, we investigated whether the differences in I_{Ca} described above could be explained by increased $Ca_V1.2$ channel unitary current amplitude. In these experiments, we recorded elementary $Ca_V1.2$ sparklets in control and BIN1-EGFP hESC-CMs at DD30. The rationale for focusing on DD30 is that at this time point $Ca_V1.2$ cluster size in control cells is similar to the one previously reported for adult myocytes (2,920 ± 151 nm^2 as indicated in Figure 3C vs. 2,555 ± 82 nm^2 [16]). Figure 5A shows TIRF images of representative control and BIN-EGFP cells loaded with the fluorescent Ca^{2+} indicator Rhod-2. The time course of $Ca_V1.2$ sparklets in the sites within the green circles is shown to the left of each image. We recorded multiple $Ca_V1.2$ sparklets in control and BIN1-EGFP cells. Figure 5B shows all-points histograms of $Ca_V1.2$ sparklet records from multiple control and BIN1-EGFP cells. The histogram from control cells was fit with a single Gaussian function with a center at 36 ± 12 nm. This corresponds to a $Ca_V1.2$ sparklet produced by the opening of a single $Ca_V1.2$ channel under similar experimental conditions [28]. In contrast, the histogram from BIN1-EGFP cells was fit with the sum of two Gaussian functions with a quantal unit of 38 ± 18 nm. Accordingly, the coupling coefficient (κ, see "Methods" section for details on how this coefficient was calculated) of $Ca_V1.2$ sparklets was 0.02 ± 0.01, which is not statistically different from zero ($p > .05$), in control cells. The coupling coefficients of $Ca_V1.2$ sparklet sites in BIN1 cells had a bimodal distribution. A subset of $Ca_V1.2$ sparklet sites in these cells had a coupling coefficient of 0.01 ± 0.0, while the other was 0.49 ± 0.03 (Fig. 5C). These data suggest that elementary $Ca_V1.2$ influx is similar in control and BIN1 cells and that the

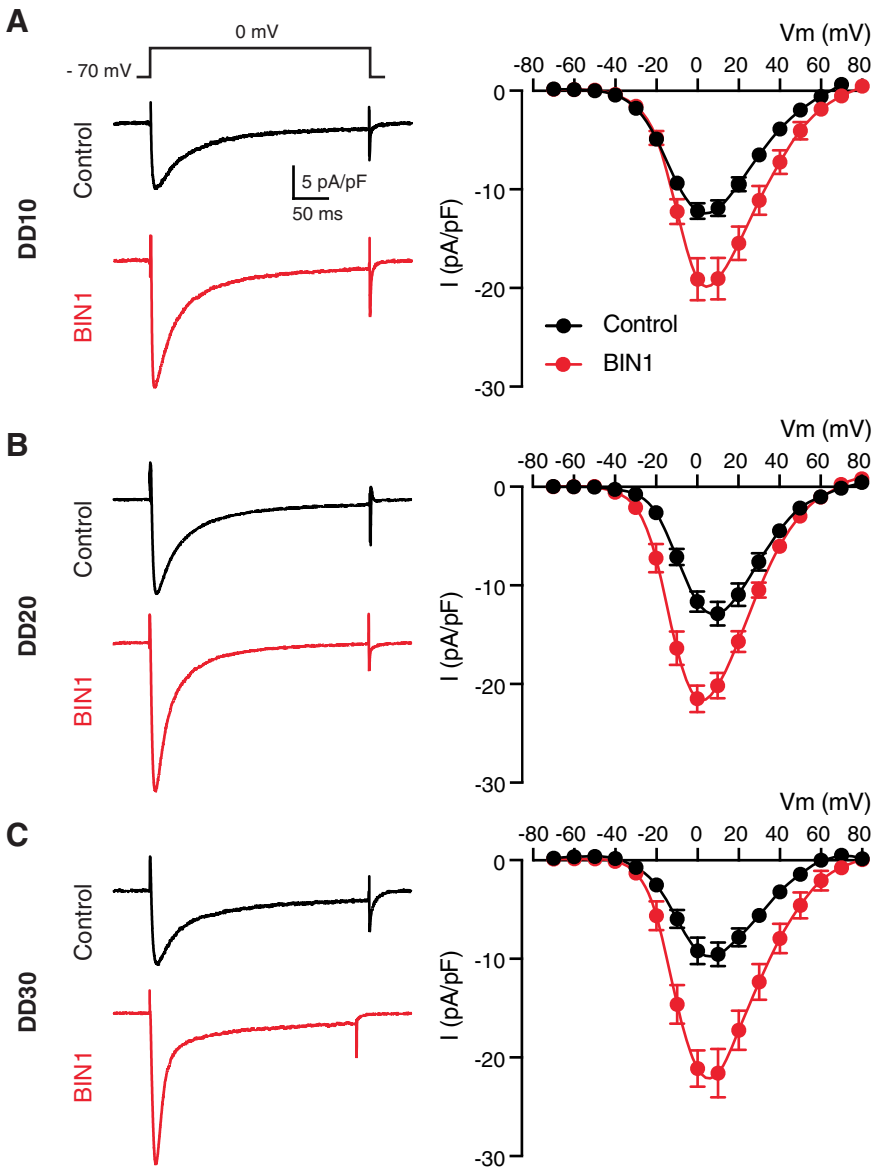

Figure 4. BIN1 increases whole-cell Ca^{2+} currents in human embryonic stem cell-derived cardiomyocyte (hESC-CM). Representative control (black) and BIN1 (red) hESC-CMs calcium currents normalized to the cell's capacitance and elicited by a 300 ms depolarizing pulse from −70 mV to +0 mV at specific differentiation days (DD) 10 **(A)**, DD20 **(B)**, and DD30 **(C)**. Right: Mean current density–voltage relationships obtained in control (n = 10 cells/DD) and BIN1 hESC-CMs (n = 10 cells/DD) from three different cell batches.

differences in I_{Ca} between these cells are due to difference in channel activity and/or number. Indeed, $Ca_V1.2$ gating in control cells and a group of $Ca_V1.2$ sparklet sites in BIN1 cells is primarily stochastic and independent, but BIN1 appears to promote coupled gating in at least a subset of channel clusters.

BIN1 Promotes Dyad Formation in hESC-CMs

Having determined that BIN1 promotes tubule formation as well as clustering and functional coupling of $Ca_V1.2$ channels, we turned our attention to the other side of the dyad: the SR. In cardiac cells, the rate of I_{Ca} Ca^{2+}-dependent inactivation has been proposed to be modulated by Ca^{2+}-dependent inactivation as a result of Ca^{2+} release from the SR [29]. Thus, studying changes in I_{Ca} can give us information on the proximity of the SR to the $Ca_V1.2$ channels and therefore the formation of dyads. We investigated the effect of BIN1 expression on the inactivation of I_{Ca}. Interestingly, BIN1 expression was associated with an increase in the rate of inactivation of I_{Ca} (Supporting Information Fig. S6). The difference was particularly evident at DD30. To quantify these apparent differences in rates of inactivation, we fit the decaying component of I_{Ca} (at 0 mV) with a two-exponential function. In control cells, the fast (τ_{fast}) and slow (τ_{slow}) time constants did not change as the cells grew older. The τ_{slow} of I_{Ca} was similar in control and BIN1 cells (DD10 p = .6547; DD20 p = .0565; DD30 p = .0824). Interestingly, the fast inactivating component of I_{Ca} in BIN1 inactivated at a faster rate than in control cells at DD10 (p = .0305), DD20 (p = .0001), and DD30 (p = .0001). Indeed, τ_{fast} decreased among BIN1 cells, being significantly faster at DD20 and DD30 than at DD10.

Then, we investigated whether local SR Ca^{2+} release contributed directly to the faster rate of inactivation observed in BIN1

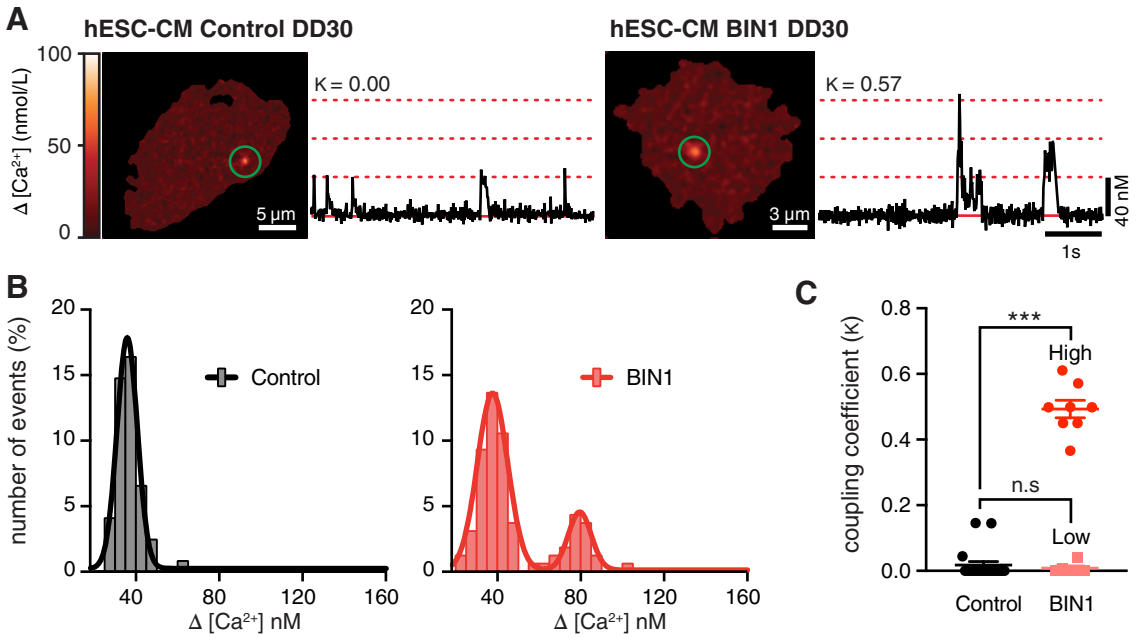

Figure 5. BIN1 increases $Ca_V1.2$ channel coupling. **(A):** TIRF images control and BIN1 human embryonic stem cell-derived cardiomyocyte (hESC-CM) at differentiation days (DD) 30, green circles show active $Ca_V1.2$ sparklets sites. Time courses of $[Ca^{2+}]_i$ in the outlined sites are shown on the right. **(B):** Event amplitude histograms of $Ca_V1.2$ sparklets recorded control (gray) and BIN1 hESC-CMs (red). The quantal amplitude of a sparklet was calculated by fitting histograms with multicomponent Gaussian functions. **(C):** Scatter plot of coupling coefficients (κ) in control (black), BIN1 high (red) and BIN1 low (light red) hESC-CMs (n = 7 cells/group). Solid lines and error bars superimposed over the individual points indicate mean ± SEM. ***, $p < .001$.

cells. For this, we compared I_{Ca} inactivation before and after application of the SR Ca^{2+} ATPase inhibitor thapsigargin (TG) to eliminate Ca^{2+} release (Supporting Information Fig. S6). In control cells, τ_{fast} and τ_{slow} did not change in response to TG treatment (Supporting Information Fig. S6A, S6B). In sharp contrast, in cells expressing BIN1, TG significantly slowed both the τ_{fast} and τ_{slow} inactivation components of I_{Ca} at DD20 and DD30 (Supporting Information Fig. S6A, S6C). These data suggest that SR Ca^{2+} release is a major contributor to I_{Ca} inactivation in BIN1 cells.

Stable Dyads are Necessary to Achieve Proper Regulation of $Ca_V1.2$ Channels by SR Calcium Release

We tested the hypothesis that BIN1 expression facilitates the formation of stable sarcolemmal-SR junctions in hESC-CMs. For this, we imaged living control or BIN1 hESC-CMs expressing a SR marker consisting of an RFP that was genetically modified to contain a N-terminal calreticulin signal sequence and a C-terminal ER retention signal, KDEL [30]. SR motility was quantified as the variance of SR-RFP fluorescence as a function of time in control and in cells coexpressing BIN1-EGFP (Supporting Information Fig. S7A). Interestingly, we found that expression of BIN1 significantly reduced SR motility as the cells matured (Supporting Information Fig. S7A). This result suggests that BIN1 plays a role in dyad formation and stabilization. The exact mechanism by which BIN1 stabilizes the SR during dyad formation remains to be elucidated. However, close examination of BIN1-EGFP and SR-RFP motility suggests that in certain regions SR and BIN1 can undergo a very close interaction. Supporting Information Figure S7B depicts a representative cell expressing BIN1-EGFP and SR-RFP. A zoom in of one of the analyzed regions is presented in Supporting Information Figure S7C; the two Airyscan super-resolution images displayed correspond to the start and end points of a 600 seconds time-lapse. The moving SR bouton is outlined by a blue line and three BIN1 clusters are labeled as C1 (green), C2 (magenta), and C3 (cyan). In this example, the SR and BIN1 clusters moved, coalescing toward the center of the image (Supporting Information Fig. S7C and Video S2). Interestingly, the velocity of the SR decreased sharply as it approached to the BIN1 clusters (Supporting Information Fig. S7D), supporting the hypothesis that BIN1 could act as an anchor for stabilizing the SR. Furthermore, studies are required to determine the identity of the SR-proteins that interact with BIN.

Taken together, our data support a role for BIN1 in clustering $Ca_V1.2$ channels (Fig. 3) along with our SR-BIN1 interaction and stabilization results, raise the intriguing possibility that expression of BIN1 could increase the number of sites where $Ca_V1.2$ and RyR come into close apposition. To test this hypothesis, we used super resolution ground state depletion (GSD) imaging to determine the spatial organization of RyRs and $Ca_V1.2$ channels in control and BIN1 cells. Figure 6A depicts representative cluster organization of $Ca_V1.2$ channels and RyR. At DD10, $Ca_V1.2$ and RyR channels were expressed into sparse clusters that rarely overlapped or were in close proximity (i.e., <50 nm). As the cells differentiated, however, the proximity of $Ca_V1.2$-RyR increased. By DD30, the number of RyR within a distance <50 nm from $Ca_V1.2$ clusters was approximately two-fold higher in BIN1 than in control cells (Fig. 6B).

BIN1 Increases $[Ca^{2+}]_i$ Transients During EC Coupling in hESC-CMs

For the last series of experiments, we investigated if the changes in tubular SR, RyR, and $Ca_V1.2$ organization in BIN1 cells were associated with changes in $[Ca^{2+}]_i$ transients. The amplitude of cell-wide $[Ca^{2+}]_i$ transients of BIN1 cells tended to be larger than control hESC-CMs at DD10 and DD20,

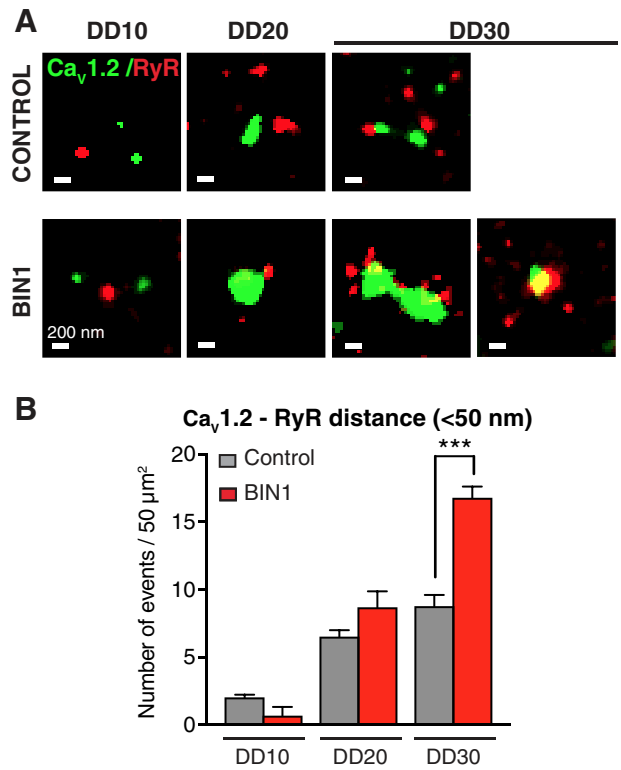

Figure 6. BIN1 expression promotes $Ca_V1.2$-RyR juxtaposition. **(A):** representative 2D GSD images of $Ca_V1.2$ (green) and RyR (red) cluster arrangements at differentiation days (DD) 10, DD20 and DD30 in control and BIN1 human embryonic stem cell-derived cardiomyocytes (hESC-CMs). **(B):** Density of RyR localized within a distance of 50 nm from $Ca_V1.2$ clusters in control (gray) and BIN1 (red) hESC-CMs (n = 4 cells/group). Data is displayed as mean ± SEM. ***, $p < .001$.

becoming statistically significant by DD30 (Fig. 7A, 7B), the day in which we found that RyR-$Ca_V1.2$ coclustering was highest in BIN1 than in control cells (Fig. 6).

We performed a more detailed analysis of these images to determine whether there were differences in the spatial dynamics of the $[Ca^{2+}]_i$ transient across BIN1 and control cells. This is important as dyads along the T-tubules synchronize SR Ca^{2+} release throughout the cell. A reasonable prediction is that in control cells without T-tubules, $[Ca^{2+}]_i$ should increase first near the sarcolemma and with a delay in the center of the cell. In BIN1 cells, however, with a T-tubular system containing numerous, stable dyads $[Ca^{2+}]_i$ is likely to increase synchronously throughout the cell.

To address these issues, we generated pseudo line-scan images from DD10, DD20, and DD30 cells and determined the time-course of $[Ca^{2+}]_i$ near the sarcolemma and in the center of hESC-CMs. Calculating the ratio between the time constant of activation at the periphery and at the center of the cells, we found that activation of the calcium transients at the center was significantly slower in control cells when compared with BIN1 cells at DD20 (p = .045) and DD30 (p = .039). Supporting our idea that cells expressing BIN1 have additional active mechanisms (i.e., T-tubules reaching to the center of the cells with functional $Ca_V1.2$-RyR channels) that contribute to the rapid increase of calcium. Figure 7D shows representative line-scans of control and BIN1 cells at DD30, where it can be seen that $[Ca^{2+}]_i$ increased first near the surface sarcolemma and, with a delay at the center of control cells (Fig. 7D; left); while in BIN1 $[Ca^{2+}]_i$ increased synchronously across the cell (Fig. 7D; right). Together with the super resolution and electrophysiological data above, these $[Ca^{2+}]_i$ data suggest that expression of BIN1 increases the number of T-tubules, $Ca_V1.2$ clusters and activity, and the number of CRUs, ultimately translating into a larger Ca^{2+} influx, SR Ca^{2+} release and synchronicity during EC coupling in hESC-CMs.

Discussion

We report multiple fundamental observations regarding the formation of T-tubules, $Ca_V1.2$ channel clusters, and dyads in developing myocytes. We show that BIN1 expression nucleates and thus promotes the formation of an extensive T-tubular network in hESC-CM. Our data suggest that $Ca_V1.2$ channels form clusters in the sarcolemma of hESC-CMs. BIN1 is expressed along the sarcolemma, where it likely functions like a delivery point for newly synthesized $Ca_V1.2$ channels, promoting the channel clustering. Tight packaging of $Ca_V1.2$ channels increase the probability of cooperative gating, enhances Ca^{2+} influx, and prolongs APs. Furthermore, BIN1 seems to serve as an anchoring point for the jSR, stabilizing CRUs, and enhancing Ca^{2+} release during EC coupling. As a result, expression of BIN1 improves the functional maturation of hESC-CM.

Our data demonstrate that overexpressing BIN1 prior to the differentiation process is sufficient for the formation of a complex network of T-tubules in hESC-CM. We followed the T-tubule formation process along cell differentiation and demonstrate that at early stages (DD10, Fig. 1), BIN1 coats small membrane invaginations that resemble those proto-tubules mentioned in the current models that explain T-tubule formation in striated muscle [31–34]. However, it remains unclear whether BIN1 acts alone or binds to other endogenous proteins such as CAV3 [6] to create these proto-tubules as suggested in the "caveolation model" [35]. Our data also demonstrates that at later time points (DD20 and DD30, Figs. 1 and 3), the proto-tubules evolve into a complex T-tubular network where $Ca_V1.2$ channels are colocalized. This finding is in agreement with the "exocytosis model" [36], which proposes that T-tubules originate and elongate at specific sites along the sarcolemma in which exocytotic vesicles are preferentially fused. Our evidence supports previous findings [15] that fusion of vesicles into T-tubules is not only supporting T-tubule growth, but has an important role in the delivery and insertion of key functional proteins such as $Ca_V1.2$ channels.

A distinguishing feature of striated muscle is that T-tubules are spaced ~1.8 µm apart, where they are anchored to Z-discs via costameres [37, 38]. It has been proposed that T-tubules are anchored to the Z-discs via a molecular complex composed of BIN1, N-WASP, and F-actin in adult myocytes [13, 39]. Yet, while hESC-CMs develop adult-like sarcomeres early after differentiation, ~90% of T-tubules do not colocalize with Z-disks, suggesting that the formation of tubules and sarcomeres in these cells is not sufficient to organize these structures as in adult myocytes. This could be due to lack of N-WASP recruitment or of another important scaffold protein required to establish the T-tubule/Z-disc connection. A follow up study

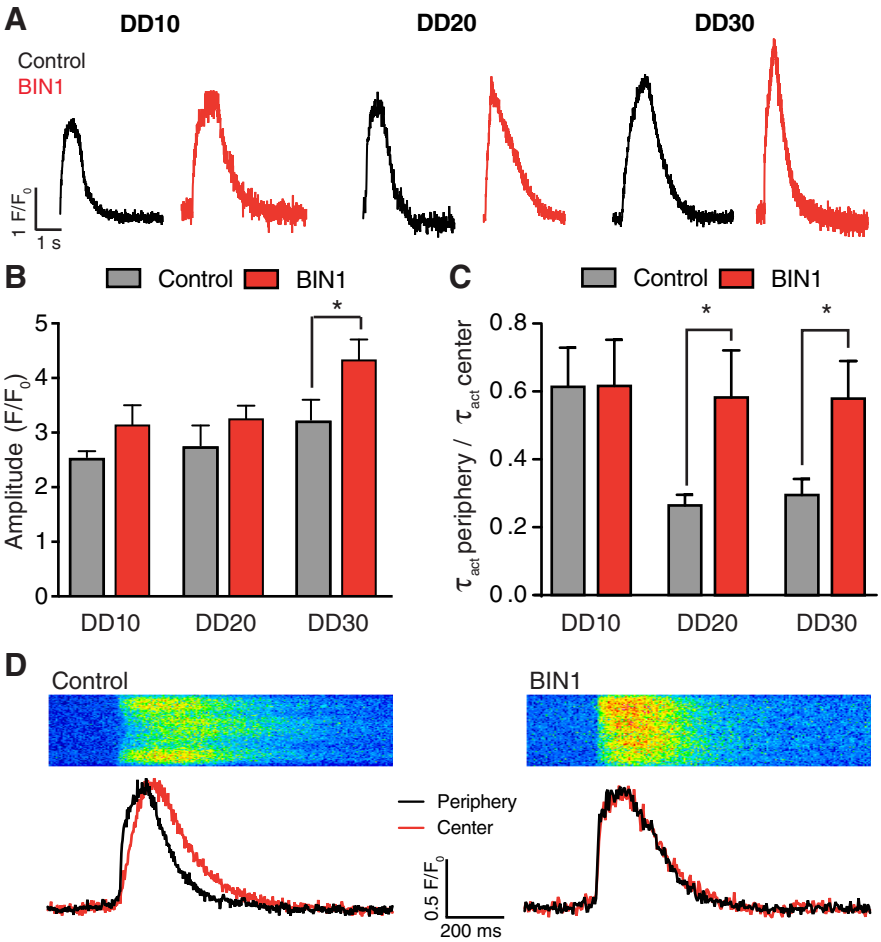

Figure 7. BIN1 increases and coordinates intracellular calcium release. **(A):** Representative spontaneous calcium transients from control (black) and BIN1 (red) human embryonic stem cell-derived cardiomyocyte (hESC-CM) cells at differentiation days (DD) 10, DD20, and DD30. **(B):** Analysis of spontaneous calcium transient peak amplitudes (n = 5–11 cells for each group; *, $p < .05$. **(C):** Ratio of the time constant of activation for the calcium transients at the periphery and center of the cells. **(D):** Above, representative confocal line-scan images of spontaneous calcium transients from control (left) and BIN1 (right) hESC-CM cells. Below, normalized calcium transients from line scan images recorded at center (red) and periphery (black) of each cell. Center time course of the control calcium transients was delayed 50 ms compared with periphery time course. Time courses at periphery and center are synchronized in BIN1 cells.

should investigate the mechanisms underlying cell-wide organization of T-tubular periodicity in cardiac muscle.

A key finding in our study is that BIN1 expression in hESC-CMs promotes clustering, cooperativity, and enhanced activity of $Ca_V1.2$ channels. Previous work from our group has revealed that the L-type $Ca_V1.2$ and $Ca_V1.3$ channels form clusters along the surface membrane of neurons, smooth muscle, and ventricular myocytes [16, 40, 41]. Here, we found that clustering of $Ca_V1.2$ channels had an important functional effect: it increased the cooperative activation of $Ca_V1.2$ channels. This is the first time that cooperative gating behavior has been positively correlated with increased channel cluster size. Not all $Ca_V1.2$ sites in BIN1 cells underwent cooperative gating, however, $Ca_V1.2$ clusters with a high coupling coefficient may be composed a relatively large number of tightly packed channels. Low activity sites are likely composed of single channels or diffused channel clysters unable to interact physically and thus open and close in a purely stochastic manner.

Di Maio et al. [42] proposed a model for the formation of CRUs in muscle in which the first step in the CRUs formation involves the formation of T-tubules. Stable sarcolemma-SR junctions are formed by JPH2. This is followed by the recruitment of the junctional proteins and channels, but could lead to "silent" dyads if these proteins fail to be delivered to these sites. We propose a modification of this model. Our data suggest that T-tubule formation and $Ca_V1.2$ clustering are early events in the formation of functional CRU. In our model, BIN1 plays a critical role in these two processes. Furthermore, by anchoring microtubules, not only does BIN1 target $Ca_V1.2$ channels to the T-tubule, but could also direct jSR movement by motors Kif5b and dynein [43] toward newly formed $Ca_V1.2$ clusters. This allows for the formation of a dyad where RyRs can be locally controlled by $Ca_V1.2$ clusters capable of gating in unison to synchronously activate CRUs throughout the cell.

For hESC-CM-based therapy to be successful, it is crucial that the transplanted cells integrate with the host cells to improve cardiac function. A well-developed T-tubule network, dyadic architecture, and functional CRUs are critical components of mature cardiomyocytes. Thus, the efforts to develop hESC-CMs with these structural and functional specializations have intensified. Indeed, as we prepared the current article for

publication, another study looking at T-tubule biogenesis but in human-induced pluripotent stem cell derived cardiomyocytes (hiPSC-CMs) was published. In this study, Parikh et al. [44] demonstrated that hiPSC-CMs develop T-tubules when exposed to thyroid and glucocorticoid hormones during differentiation. This was not associated with an increase in BIN1 expression, suggesting a BIN1-independndent mechanism for T-tubular formation. A future study should investigate whether a combination of BIN1 expression and thyroid/glucocorticoid hormone treatment would synergistically create T-tubule networks like those in adult cardiomyocytes.

Our study has some limitations, such as using a heterogeneous population of hESC-CMs. Although creating a stable clone would be ideal and provide more homogeneous outcomes, we have been limited by the sensitivity of the hESCs toward approaches needed to create a homogenous population such as flow cytometry-based cell sorting, clonogenicity assay or antibiotic selection. However, we implemented spontaneous contraction (in control cells) and contraction plus GFP expression (in BIN1) as strict experimental selection criteria. A question raised by our work is whether fusion of BIN1 to EGFP altered the function of this scaffolding protein, confounding interpretation of our data. Two observations suggest this is not likely the case. First, hESC-CMs expressing BIN1-EGFP exhibit a more developed T-tubule network. Second, BIN1-EGFP expression also increased expression of $Ca_V1.2$ channels in hESC-CMs. These findings recapitulate previously proposed roles of BIN1 in adult myocytes [13, 15], and thus indicate that use of a BIN1-EGFP fusion protein does not exert any extraneous effects on BIN1 protein conformation or function. To conclude, future studies should involve validation of the major results from this study on other hESC as well as human iPSC lines as means to determine the capacity of BIN1 to induce T-tubules and CRU formation in multiple cell lines. Additionally, a follow up study incorporating engineered endonucleases such as transcription activator-like effector nucleases or clustered regularly interspaced short palindromic repeat will provide virus-free approaches to overexpress BIN1 [45]. Recent advancements in CRISPR technology also enable BIN1 overexpression using translationally relevant, DNA-free, RNA-guided Cas9 ribonucleoprotein-based approaches that may be used for future studies and to enhance the maturation of cardiomyocytes derived from pluripotent stem cells [46]. Finally, the creation of a stable hESC-CM population could lead to lower variability in T-tubular development as well as AP waveforms upon induction of BIN1 expression.

Conclusion

We report multiple fundamental observations regarding the formation of T-tubules, $Ca_V1.2$ channel clusters, and dyads in developing myocytes. We show that BIN1 expression nucleates and thus promotes the formation of an extensive T tubular network in hESC-CM. Our data suggest that $Ca_V1.2$ channels form clusters in the sarcolemma of hESC-CMs. BIN1 is expressed along the sarcolemma, where it likely functions like a delivery point for newly synthesized $Ca_V1.2$ channels, promoting the channel clustering. Tight packaging of $Ca_V1.2$ channels increase the probability of cooperative gating, enhances Ca^{2+} influx, and prolongs APs. Furthermore, BIN1 seems to serve as an anchoring point for the jSR, stabilizing CRUs, and enhancing Ca^{2+} release during EC coupling. As a result, expression of BIN1 improves the functional maturation of hESC-CM.

Acknowledgments

We thank Eric Arreola, Sean Woods, and Dellaney Rudolph-Gandy for technical assistance. This work was supported by grants from the U.S. National Institutes of Health (NIH): R01-HL085686 (L.F.S.) and 1K99AG056595-01 (C.M.M.); the American Heart Association: 15SDG25560035 (R.E.D.) and 16SDG30970046 (N.H.).

Author Contributions

L.F.S.: conception and design, financial support, data analyses and interpretation, manuscript writing, final approval of manuscript; C.M.M.: conception and design, financial support, collection and assembly of data, data analyses and interpretation, manuscript writing, final approval of manuscript; A.D.L.M.: conception and design, collection and assembly of data, data analyses and interpretation, manuscript writing; S.T., S.O., C. M.: collection and assembly of data, data analyses and interpretation; N.H.: collection and assembly of data, data analyses and interpretation, manuscript writing, financial support; R.E. D.: financial support, data analyses and interpretation, manuscript writing.

Disclosure of Potential Conflicts of Interest

The authors indicated no potential conflicts of interest.

References

1 Chong JJ, Yang X, Don CW et al. Human embryonic-stem-cell-derived cardiomyocytes regenerate non-human primate hearts. Nature 2014;510:273–277.

2 Quijada P, Salunga HT, Hariharan N et al. Cardiac stem cell hybrids enhance myocardial repair. Circ Res 2015;117:695–706.

3 Bolli R, Ghafghazi S. Stem cells: Cell therapy for cardiac repair: What is needed to move forward? Nat Rev Cardiol 2017;14: 257–258.

4 Soeller C, Cannell MB. Numerical simulation of local calcium movements during L-type calcium channel gating in the cardiac diad. Biophys J 1997;73:97–111.

5 Gomez AM, Valdivia HH, Cheng H et al. Defective excitation–contraction coupling in experimental cardiac hypertrophy and heart failure. Science 1997;276:800–806.

6 Galbiati F, Engelman JA, Volonte D et al. Caveolin-3 null mice show a loss of caveolae, changes in the microdomain distribution of the dystrophin–glycoprotein complex, and T-tubule abnormalities. J Biol Chem 2001;276: 21425–21433.

7 Murphy RM, Mollica JP, Lamb GD. Plasma membrane removal in rat skeletal muscle fibers reveals caveolin-3 hot-spots at the necks of transverse tubules. Exp Cell Res 2009;315:1015–1028.

8 Zampighi G, Vergara J, Ramon F. On the connection between the transverse tubules and the plasma membrane in frog semitendinosus skeletal muscle. Are caveolae the mouths of the transverse tubule system? J Cell Biol 1975;64:734–740.

9 Chase TH, Cox GA, Burzenski L et al. Dysferlin deficiency and the development of cardiomyopathy in a mouse model of limb-girdle muscular dystrophy 2B. Am J Pathol 2009; 175:2299–2308.
10 Demonbreun AR, Rossi AE, Alvarez MG et al. Dysferlin and myoferlin regulate transverse tubule formation and glycerol sensitivity. Am J Pathol 2014;184:248–259.
11 Beavers DL, Landstrom AP, Chiang DY et al. Emerging roles of junctophilin-2 in the heart and implications for cardiac diseases. Cardiovasc Res 2014;103:198–205.
12 Chopra N, Yang T, Asghari P et al. Ablation of triadin causes loss of cardiac Ca^{2+} release units, impaired excitation–contraction coupling, and cardiac arrhythmias. Proc Natl Acad Sci USA 2009;106:7636–7641.
13 Hong T, Yang H, Zhang SS et al. Cardiac BIN1 folds T-tubule membrane, controlling ion flux and limiting arrhythmia. Nat Med 2014;20:624–632.
14 Muller AJ, Baker JF, DuHadaway JB et al. Targeted disruption of the murine Bin1/Amphiphysin II gene does not disable endocytosis but results in embryonic cardiomyopathy with aberrant myofibril formation. Mol Cell Biol 2003;23:4295–4306.
15 Hong TT, Smyth JW, Gao D et al. BIN1 localizes the L-type calcium channel to cardiac T-tubules. PLoS Biol 2010;8:e1000312.
16 Dixon RE, Moreno CM, Yuan C et al. Graded Ca(2)(+)/calmodulin-dependent coupling of voltage-gated CaV1.2 channels. Elife 2015;4:e05608.
17 Dixon RE, Yuan C, Cheng EP et al. Ca^{2+} signaling amplification by oligomerization of L-type $Ca_V1.2$ channels. Proc Natl Acad Sci USA 2012;109:1749–1754.
18 Palpant NJ, Hofsteen P, Pabon L et al. Cardiac development in zebrafish and human embryonic stem cells is inhibited by exposure to tobacco cigarettes and e-cigarettes. PLoS ONE 2015;10:e0126259.
19 Hariharan N, Quijada P, Mohsin S et al. Nucleostemin rejuvenates cardiac progenitor cells and antagonizes myocardial aging. J Am Coll Cardiol 2015;65:133–147.
20 Gentet LJ, Stuart GJ, Clements JD. Direct measurement of specific membrane capacitance in neurons. Biophys J 2000;79:314–320.
21 Maltsev VA, Wobus AM, Rohwedel J et al. Cardiomyocytes differentiated in vitro from embryonic stem cells developmentally express cardiac-specific genes and ionic currents. Circ Res 1994;75:233–244.
22 Pasqualin C, Gannier F, Malecot CO et al. Automatic quantitative analysis of T-tubule organization in cardiac myocytes using ImageJ. Am J Physiol Cell Physiol 2015;308: C237–C245.
23 Matsa E, Rajamohan D, Dick E et al. Drug evaluation in cardiomyocytes derived from human induced pluripotent stem cells carrying a long QT syndrome type 2 mutation. Eur Heart J 2011;32:952–962.
24 Saggin L, Gorza L, Ausoni S et al. Troponin I switching in the developing heart. J Biol Chem 1989;264:16299–16302.
25 Westfall MV, Samuelson LC, Metzger JM. Troponin I isoform expression is developmentally regulated in differentiating embryonic stem cell-derived cardiac myocytes. Dev Dyn 1996;206:24–38.
26 Hong TT, Smyth JW, Chu KY et al. BIN1 is reduced and Cav1.2 trafficking is impaired in human failing cardiomyocytes. Heart Rhythm 2012;9:812–820.
27 Sato D, Dixon RE, Santana LF et al. A model for cooperative gating of L-type Ca^{2+} channels and its effects on cardiac alternans dynamics. PLoS Comput Biol 2018;14: e1005906.
28 Navedo MF, Amberg GC, Votaw VS et al. Constitutively active L-type Ca^{2+} channels. Proc Natl Acad Sci USA 2005;102: 11112–11117.
29 Adachi-Akahane S, Cleemann L, Morad M. Cross-signaling between L-type Ca^{2+} channels and ryanodine receptors in rat ventricular myocytes. J Gen Physiol 1996;108: 435–454.
30 Vega AL, Yuan C, Votaw VS et al. Dynamic changes in sarcoplasmic reticulum structure in ventricular myocytes. J Biomed Biotechnol 2011;2011:382586.
31 Martonosi A. *The Development of the Sarcoplasmic Reticulum*. Amsterdam: Hardwood Academic Publishers, 2000.
32 Franzini-Armstrong C. Fine structure of sarcoplasmic reticulum and tranverse tubular system in muscle fibers. Fed Proc 1964;23: 887–895.
33 Lindner E. Submicroscopic morphology of the cardiac muscle. Z Zellforsch Mikrosk Anat 1957;45:702–746.
34 Huxley HE. Evidence for continuity between the central elements of the triads and extracellular space in frog sartorius muscle. Nature 1964;202:1067–1071.
35 Ishikawa H. Formation of elaborate networks of T-system tubules in cultured skeletal muscle with special reference to the T-system formation. J Cell Biol 1968;38:51–66.
36 Schiaffino S, Cantini M, Sartore S. T-system formation in cultured rat skeletal tissue. Tissue Cell 1977;9:437–446.
37 Hong T, Shaw RM. Cardiac T-tubule microanatomy and function. Physiol Rev 2017;97:227–252.
38 Bloch RJ, Capetanaki Y, O'Neill A et al. Costameres: Repeating structures at the sarcolemma of skeletal muscle. Clin Orthop Relat Res 2002;403:S203–S210.
39 Falcone S, Roman W, Hnia K et al. N-WASP is required for Amphiphysin-2/BIN1-dependent nuclear positioning and triad organization in skeletal muscle and is involved in the pathophysiology of centronuclear myopathy. EMBO Mol Med 2014;6: 1455–1475.
40 Moreno CM, Dixon RE, Tajada S et al. Ca (2+) entry into neurons is facilitated by cooperative gating of clustered CaV1.3 channels. Elife 2016;5:e15744.
41 Vivas O, Moreno CM, Santana LF et al. Proximal clustering between BK and CaV1.3 channels promotes functional coupling and BK channel activation at low voltage. Elife 2017;6:e28029.
42 Di Maio A, Karko K, Snopko RM et al. T-tubule formation in cardiacmyocytes: Two possible mechanisms? J Muscle Res Cell Motil 2007;28:231–241.
43 Vega AL, Santana LF. Dynamic changes in sarcoplasmic reticulum structure in ventricular myocytes. J Biomed Biotechnol 2011; 2011:1–14.
44 Parikh SS, Blackwell DJ, Gomez-Hurtado N et al. Thyroid and glucocorticoid hormones promote functional T-tubule development in human-induced pluripotent stem cell derived cardiomyocytes. Circ Res 2017; 121:1323–1330.
45 Lee JG, Sung YH, Baek IJ. Generation of genetically-engineered animals using engineered endonucleases. Arch Pharm Res 2018; 41:885–897.
46 Shin J, Lee N, Cho S et al. Targeted genome editing using DNA-free RNA-guided Cas9 ribonucleoprotein for CHO cell engineering. Methods Mol Biol 2018;1772:151–169.

See www.StemCells.com for supporting information available online.